

pubs.acs.org/crystal Article

Monolithic Growth of Patternable III—V on LiNbO₃

Hyun Uk Chae, [†] Zezhi Wu, [†] Yiyan Yu, Hee gon Kim, Juan Sanchez Vazquez, Chun-Ho Lee, Mengji Yu, and Rehan Kapadia*



Cite This: *Cryst. Growth Des.* 2024, 24, 4466–4472



ACCESS More Article Recommendations Supporting Information

LINDO3 InP

LINDO3 LINDO3 Z

ABSTRACT: Developing cost-effective III–V integration has posed a critical challenge in integrated photonics. To date, the integration of III–V with LiNbO $_3$ has been demonstrated through epitaxial transfer or wafer bonding; however, challenges persist in terms of both cost and alignment. In this paper, we demonstrated various patterned single-crystalline III–V mesas achieved through low-temperature templated liquid-phase (LT-TLP) growth on LiNbO $_3$. Both electrical and optical characterizations reveal the distinctive quality of III–V even without using lattice-matched substrates. InAs on LiNbO $_3$ shows high electron mobility (2500 cm²/V·s) at room temperature, while InP on LiNbO $_3$ displays uniform photoluminescence and the ability to tune the optical properties of the grown material through in situ doping. We project that the reported LT-TLP monolithic III–V growth on LiNbO $_3$ reported here will prove beneficial in designing photonic devices such as photon generation and detection or gain materials.

INTRODUCTION

In recent years, the advancement of integrated optical components has focused on exploring and integrating diverse material classes in the pursuit of selecting the ideal material for a given functionality and then integrating disparate materials to create highly efficient photonic devices with complex behaviors. 1-4 The integrated photonic integrated circuit (PIC) comprises two crucial elements: (i) waveguiding materials, responsible for transporting light within the circuit with minimal losses, and (ii) materials for photon generation and detection. LiNbO₃, with its large transparency window spanning from ultraviolet to mid-infrared wavelengths and a substantial Pockels coefficient of 32 pm V⁻¹, has emerged as a key material of interest, enabling efficient, low-driving voltage and high-speed electro-optic (EO) modulators in an optical fiber platform. After LiNbO₃ on insulator wafers became available through wafer bonding and smart-cut techniques, many EO and nonlinear integrated PIC devices were demonstrated utilizing very low-loss optical waveguides with 2.7 dB/m.^{5-10}

While the second component is dedicated to photon detection and generation, III-V materials have taken the center stage due to their extensive study and dominance. This

is attributed to their flexibility in engineering band gaps and exhibiting high carrier mobility compared to other materials. 11-14 Consequently, III–V materials have become integral in creating sources, detectors, and high-speed electronic devices. 15-17 Although III–V semiconductors through wafer bonding on LiNbO₃ have replicated most optical functions demonstrated in nonepitaxial platforms, their performance has often been compromised by material constraints and compatibility issues. 18-21 Flip-chip bonding and edge coupling were employed to integrate the photonic source into the LiNbO₃; however, coupling losses and alignment issues remained. 22,23 The efforts have been directed toward realizing monolithic PICs, where all the components can be grown and fabricated within a single platform. The ideal scenario involves creating monolithic PICs that integrate cutting-edge devices

Received: January 25, 2024 Revised: May 10, 2024 Accepted: May 13, 2024 Published: May 28, 2024





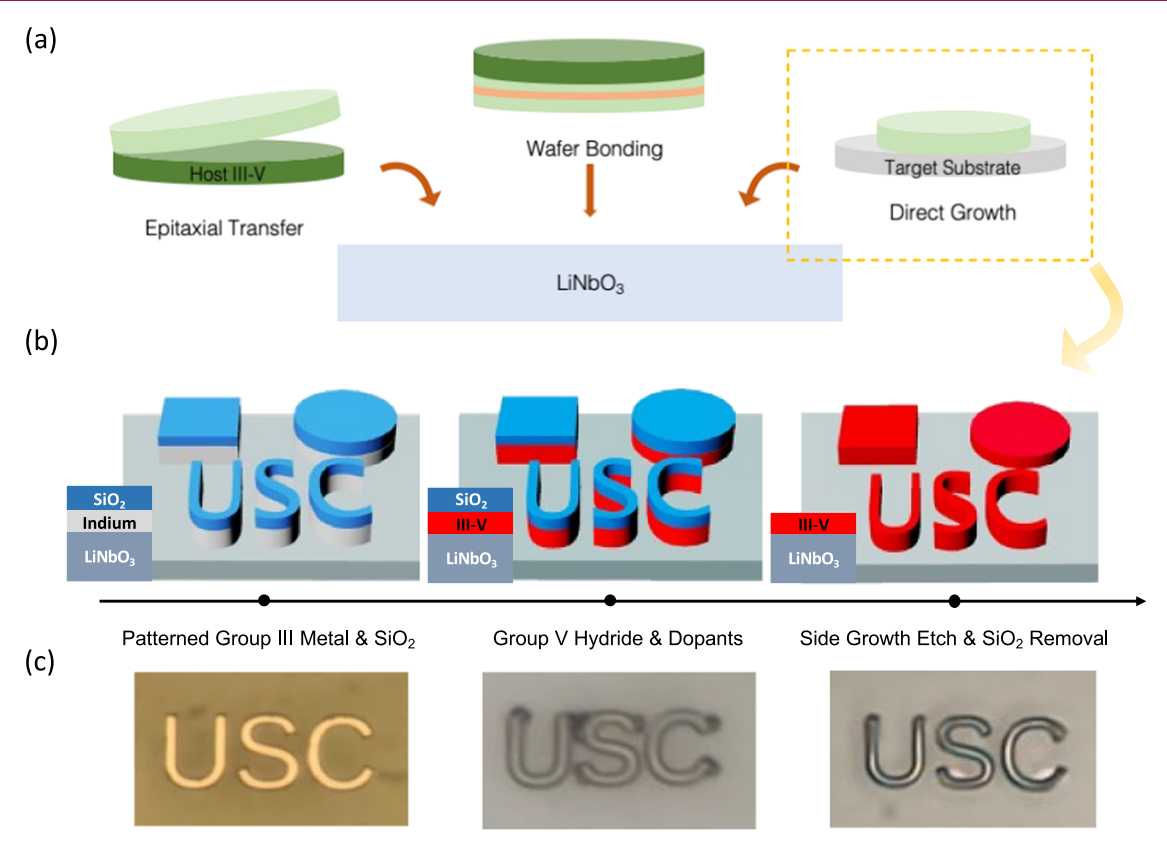


Figure 1. (a) Schematic of different approaches to integrate III–V onto a LiNbO₃ platform. (b) 3D schematic process flow of templated liquid-phase growth of III–V on LiNbO₃. The cross-section of the material stack shown in the 2D figure. (c) Optical microscopy images of liquid indium to fully grown III–V on LiNbO₃.

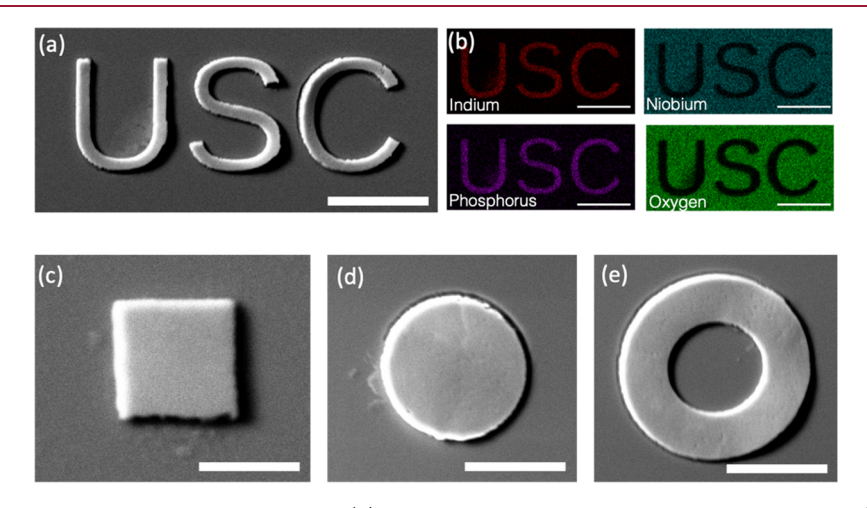


Figure 2. (a) SEM image of patterned InP with the letter USC. (b) EDS map of InP grown on LiNbO₃. SEM images of (c) square shape, (d) circle shape, and (e) ring shape of InP. Scale bar: 5 μ m.

from each material group; however, the inherent disparities between these materials have made this goal less feasible.

This study presents the first successful monolithic growth of a III–V semiconductor on LiNbO₃ using a recently developed low-temperature templated liquid-phase (LT-TLP) growth.^{24,25} The feasibility of growing various patterns of III–V has been experimentally verified. This achievement opens new prospects for designing innovative, efficient, and cost-effective photonic devices.

DISCUSSION

Figure 1a illustrates a schematic representation of various strategies for integrating III—V on a LiNbO₃ substrate. Owing to lattice mismatch, achieving a single-crystalline epitaxial layer of III—V on LiNbO₃ using conventional growth methods is not viable. Our research group has recently demonstrated the feasibility of single-crystalline III—V growth on nonepitaxial substrates through LT-TLP. ^{24,25} This growth process is specifically conducted at temperatures below 400 °C, making it compatible with the back end of the line (BEOL) process and suitable for constructing a PIC on a complementary

Crystal Growth & Design pubs.acs.org/crystal Article

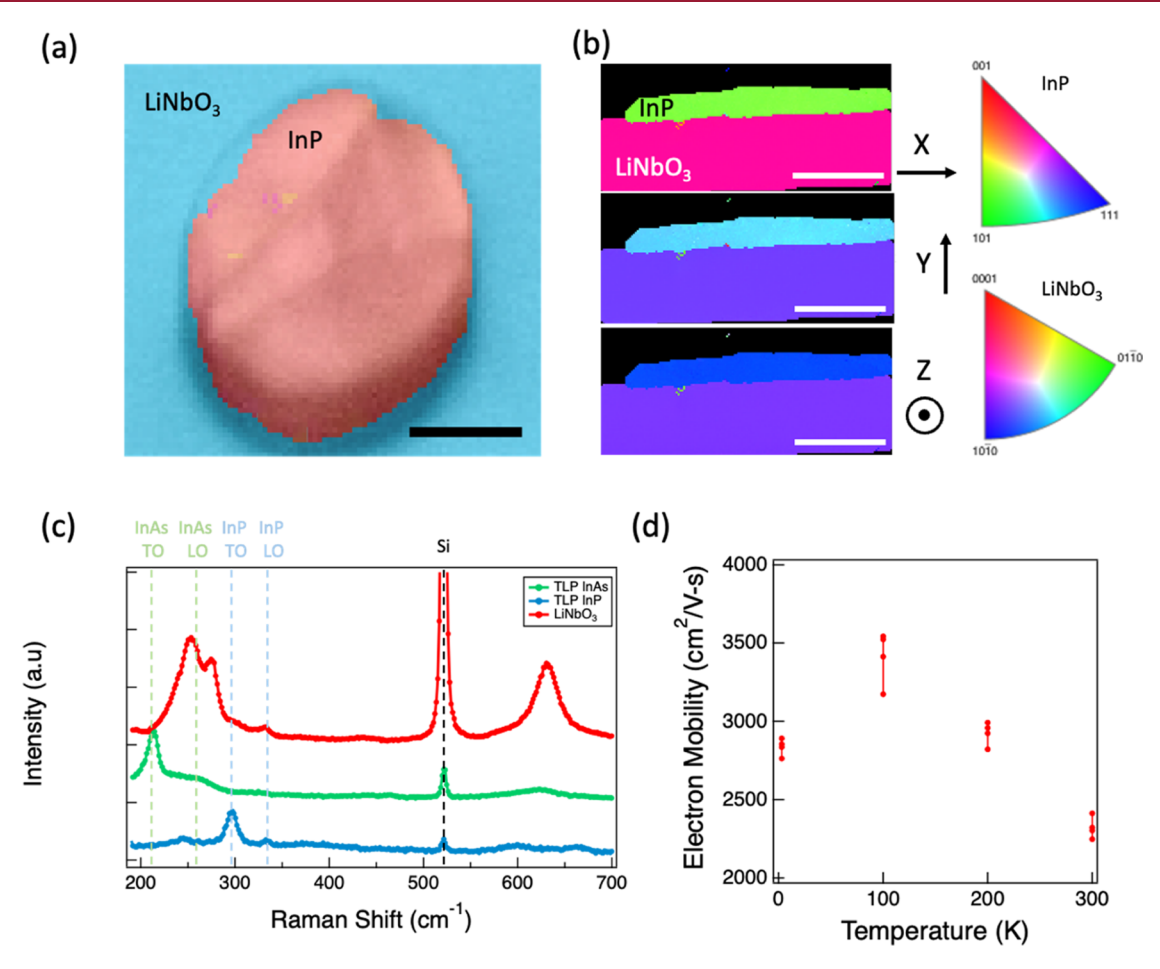


Figure 3. (a) EBSD on circle shape InP on LiNbO₃. Scale bar = $3 \mu m$. (b) TKD pattern of InP on LiNbO₃. Scale bar: 500 nm. (c) Raman spectrum of InP and InAs on LiNbO₃. (d) Hall mobility of InAs in different temperature ranges.

metal-oxide-semiconductor (CMOS) platform. 26,27 While previous work has demonstrated the feasibility of growing III-V on nonepitaxial substrates, such as amorphous dielectrics and metals, the significance of our work lies in two key aspects: (i) providing experimental evidence that a similar approach is effective for emerging photonic materials and (ii) developing a patternable III-V with various doping conditions on LiNbO₃. This material can serve as an epi-ready site for subsequent epitaxial processes. The monolithic growth approach presents two primary advantages over epitaxial transfer methods for III-Vs. First, it obviates the need for expensive epitaxial III-Vs, thereby reducing costs. Second, transfer-based approaches for III-Vs are constrained by the limited size of epitaxial substrates, thus failing to overcome the barrier to potential large area applications in silicon-compatible processes. Figure 1b presents a schematic representation of the LT-TLP growth process on LiNbO₃, with details in the Methods Section and Supporting Information Figure 1. In summary, a group III metal (indium or gallium) and a silicon dioxide capping layer are precisely deposited in the desired template geometry and pattern onto LiNbO₃ through evaporation. Subsequently, the substrate undergoes heating in a H₂ environment, causing the group III metal to melt into a liquid phase thanks to the low melting point. At the growth temperature, a precursor gas is introduced, leading to supersaturation and precipitation of the target material, in this case, InP and InAs, although the method is not limited exclusively to In-based III-Vs. Notably, commencing with the prepatterned group III metal allows the

definition of the III—V shape according to diverse device applications. Precursor flux control facilitates single nucleation at the pattern, resulting in single-crystalline growth. ²⁸ Figure 1c shows optical microscope images of the progression from liquid indium to the fully grown InP in the shape of the letters *USC*

The versatility of growing varied patterns on LiNbO3 is pivotal in constructing practical integrated photonic elements. Figure 2a displays a scanning electron microscopy (SEM) image of the III-V growth in the USC letter, demonstrating a sharp, smooth surface without a lattice-matched substrate. Figure 2b exhibits the corresponding energy-dispersive spectrometry (EDS) maps of In, P, Nb, and O, crucially revealing a clean boundary between InP and the underlying LiNbO₃ substrate. Supporting Information Figure 2 shows the cross-sectional SEM and corresponding EDS for the material stacks. The EDS result of InAs in the same shape is also shown in Supporting Information Figure 3. Our endeavors in LT-TLP growth has encompassed diverse III-V shapes, as illustrated in Figure 2c-e, showing square, circle, and ring configurations. These varied patterns hold promise for future applications, such as utilizing nano/micropatterns of circles as platforms for whispering gallery mode lasers.^{29,30} The square shape holds potential utility as a platform for a photodetector, creating additional junctions atop it. Alternatively, it can serve as a metasurface due to the high refractive index of III-V materials. The ring-shaped III-V configuration may find application in ring resonator integration. However, the efficacy of these

Crystal Growth & Design pubs.acs.org/crystal Article

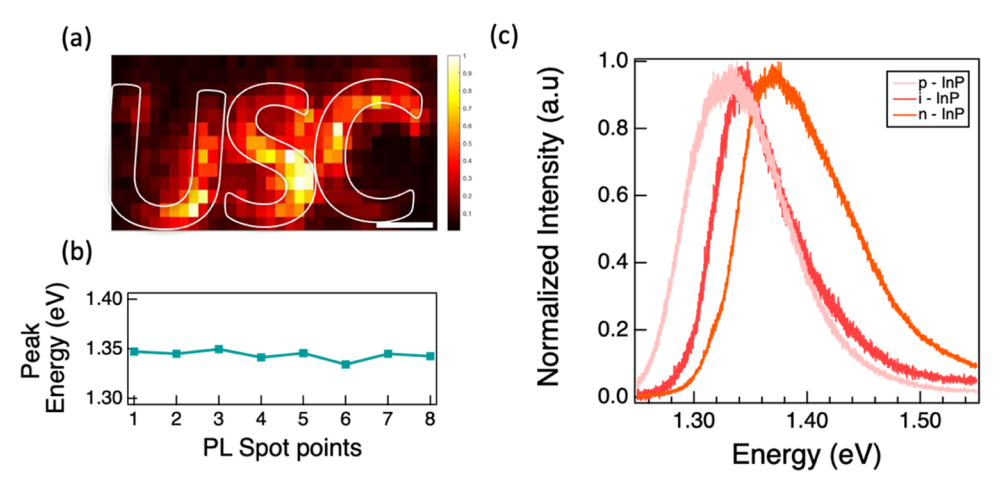


Figure 4. (a) PL mapping of InP having the USC letter at a peak energy of 1.34 eV; scale bar: 2 μ m. (b) Peak energy of PL from different InP spots. (c) PL from different InPs grown under doped conditions.

applications hinges on the quality of the material used as an efficient photonic component. In particular, when the grown III–V material is polycrystalline or amorphous, the quality of the material is not sufficient for any applications.

To assess the crystallinity of our material grown on LiNbO₃, we conducted a characterization of the microstructural crystallographic orientation using electron backscatter diffraction (EBSD). In EBSD, each color corresponds to a distinct out-of-plane orientation. Therefore, an LT-TLP layer with a single color indicates a single crystallinity. Figure 3a depicts the EBSD map of the circle-shaped III-V structures, revealing a single out-of-plane crystal orientation in the grown material. LiNbO₃, bonded from the bulk wafer to the SiO₂/Si wafer before the growth of any III-V on top, also exhibits single crystallinity. A transmission Kikuchi diffraction (TKD) pattern of the material along the entire cross-sectional length was obtained to characterize the interface between two singlecrystalline materials. An inverse pole figure (IPF) in the x,y,zdirection shown in Figure 3b illustrates that the grown InP is single-crystalline on top of single-crystalline LiNbO₃. The Raman spectrum of LT-TLP-grown InP and InAs presented in Figure 3c identifies discernible transverse (TO) and longitudinal (LO) mode peaks. For InAs, these peaks are observed at 218 cm⁻¹ (TO) and 239 cm⁻¹ (LO), while for InP, peaks are noted at 300 cm⁻¹ (TO) and 348 cm⁻¹ (LO). 31,32 Additionally, the Raman spectrum exhibits peaks corresponding to LiNbO₃, aligning with findings from prior studies on LiNbO₃.³³ Alongside the crystalline validation, the electron mobility of the III and V templated films is determined through Hall effect measurements. In this context, InAs, characterized by higher electron mobility, is selected over InP for mobility extraction. Recently, studies have shown that acoustoelectric interactions of propagating phonons and electrons lead to the nonreciprocal amplification of radio frequency (RF) acoustic waves, creating an amplifier with the integration of a high-electron mobility semiconductor on LiNbO₃.^{34,35} The material integration in the aforementioned studies was executed through a transfer method. This emphasizes the substantial potential of monolithic III-V integration. Figure 3d illustrates the mobility profile of a representative InAs Hall element. A peak mobility of 3600 cm²/V·s is recorded at 100 K, while the room-temperature mobility under these conditions is approximately 2500 cm²/V· s with a carrier concentration of $\sim 10^{17}$ cm⁻³. The characteristic

curve shape aligns with that of a typical single-crystal 3D semiconductor. So, 37 In addition, theoretical calculation using temperature-dependent scattering components such as ionized impurities and phonon scattering also explains the behavior of the experimental data of the mobility measurement. Given that our grown III—V is a single-crystalline semiconductor, the primary factor influencing the mobility is temperature-independent components such as surface roughness scattering or crystalline defects, and the mobility of TLP III—V can be further improved with growth optimization to improve surface roughness and crystalline quality.

Material quality assessment is a critical aspect of semiconductor analysis, with photoluminescence (PL) serving as a key factor. The presence of low-quality or defective materials can lead to nonradiative recombination, a pivotal consideration in the fabrication of optoelectronic and photonic devices. Steady-state photoluminescence (PL) mapping of LT-TLP InP with the USC shape on LiNbO3 is presented in Figure 4a. The PL mapping reveals illumination of the PL signal from the USC shape, while the substrate remains dark, illustrating a distinct contrast between the two materials. The variation of the PL signal within USC InP comes from two different growth factors; (i) background doping from Si through SiO₂ capping layer decomposition during the growth and carbon contamination in the growth system and (ii) the growth temperature. We have experimentally proved that the uniformity of material quality heavily depends on the growth temperature.²⁴ However, the growth approach does not limit the material intrinsic quality but is more related to the growth parameters that can be tuned in future work such as chamber conditions and growth temperatures. Figure 4b displays the distribution of the peak energy of PL from eight different spots within the material, demonstrating a uniform distribution that indicates the consistency of the material grown on top of LiNbO₃.

In semiconductor growth processes, precise control over doping levels is imperative for constructing various junctions to create functional devices. Given that the LT-TLP process lacks inherent acceptor or donor atoms during normal growth, dopants were introduced during LT-TLP growth by using external precursors. Silane (SiH₄) was incorporated during growth to introduce silicon as a donor, while trimethylaluminum (DEZn) was introduced as an acceptor for III–V semiconductors. Figure 4c presents the normalized PL signal from three material groups with intrinsic, n-type, and p-type

InP. In doped semiconductors, band gap widening (BGW) occurs due to occupied lower states in the conduction band, while band gap narrowing (BGN) results from many-body interactions on doping. Both n-type and p-type InP grown by LT-TLP exhibit shifts in PL signals with opposite directions, where p-InP demonstrates a *red shift* (1.33 eV) and n-InP exhibits a *blue shift* (1.37 eV). While both BGN and BGW contribute to shifting the effective band gap, the prominence of BGW is observed in n-InP, where the effective mass of the electron ($m_e^* = 0.08 \, m_0$) is approximately 1 order lighter than that of the heavy hole in InP ($m_h^* = 0.6 \, m_0$). This phenomenon induces a higher impact of BGW in n-type InP, as evidenced by the PL signal.

CONCLUSIONS

In conclusion, this work has comprehensively explored advancements in integrated optical components, specifically combining III-V materials on LiNbO3 to construct highly efficient PICs. It is shown that the monolithic growth of III-V on LiNbO3 through LT-TLP growth can precisely control the desired pattern. Notably, single-crystalline III-V was achieved on LiNbO₃ despite the growth on a nonepitaxial substrate. EBSD confirms the crystallinity of the grown InP and InAs. Hall mobility measurement, PL, and Raman spectroscopy were employed to investigate the electrical and optical properties. The demonstrated doping of III-V opens possibilities for potential monolithic on-chip III-V devices on LiNbO3, including p-n/p-i-n junctions in stacked or lateral growth configurations. Doped LT-TLP III-V can serve as an epi-ready spot for subsequent homo/heteroepitaxial III-V growth, enabling the development of various quantum structures through MBE or MOCVD. We believe that this novel approach to integrate III-V materials on LiNbO₃ on an insulator platform will pave the way to realizing various semiconductor-based lasers and photodetectors with versatile scalability.44-47

■ METHODS

Patternable III-V TLP Growth on LiNbO₃. A LiNbO₃ bonded to the SiO₂/Si substrate was first degreased by rinsing with acetone, IPA, and DI water for 30 s each. Desired patterns were written by conventional photolithography with a Heidelberg direct writer (DWL 66) or E-beam lithography (Raith EBPG 5150). Indium was evaporated by thermal evaporation, while the sample stage was cooled with a liquid nitrogen flow (-185 °C) to minimize the roughness of the indium template. LT-TLP was carried out in a Thomas Swan CCS MOCVD. Arsine (AsH₃) or phosphine (PH₃) with H2 as the carrier gas was used to fully grow the III-V without using metal-organic sources such as TMIn or TMGa. The growth pressure was 76 Torr, with 50 sccm of group V hydride gases with a 500 sccm H₂ flow. Dopant precursors are trimethylaluminum (DEZn) for the p-dopant and silane (SiH₄) for the n-dopant with 5 sccm flow rate. After LT-TLP III-V growth, unnecessary side growth was removed by Cl₂ ICP-RIE etch while using the SiO₂ capping layer as a dry etch mask. The SiO₂ capping layer was removed with the HF etchant.

Scanning Electron Microscopy and Focused Ion Beam. Scanning electron microscopy images were obtained using a Nova NanoSEM 450 and a Helios G4 PFIB field-emission scanning electron microscope. A focused ion beam (FIB) attached to the Helios G4 PFIB was used to analyze the cross-section of the GaAs MSM structure. EBSD was carried out by an Oxford detector attached to the Helios G4 PFIB system under a 70° pretilted stage.

Hall Mobility Measurement. Mobility measurements are conducted across different temperature ranges (2-300 K) utilizing

a physical property measurement system (PPMS) with a Hall bar shape pattern.

Photoluminescence and Raman Spectral Measurement. Steady-state photoluminescence measurements were carried out in a Renishaw inVia confocal Raman microscope setup using a constant-power 532 nm laser source as the excitation and a Si CCD detector. For the PL heat map, a peak position at 1.34 eV was selected, and the pixel size for PL signal collection was defined as a 500 nm window.

ASSOCIATED CONTENT

Data Availability Statement

The data supporting the plots within this paper and other study findings are available from the corresponding author upon reasonable request.

Supporting Information

The Supporting Information is available free of charge at https://pubs.acs.org/doi/10.1021/acs.cgd.4c00116.

LT-TLP growth process flow and cross-sectional EDS of InP and EDS of InAs on LiNbO₃ (PDF)

AUTHOR INFORMATION

Corresponding Author

Rehan Kapadia — Ming Hsieh Department of Electrical and Computer Engineering, University of Southern California, Los Angeles, California 90089, United States; orcid.org/0000-0002-7611-0551; Email: rkapadia@usc.edu

Authors

Hyun Uk Chae — Ming Hsieh Department of Electrical and Computer Engineering, University of Southern California, Los Angeles, California 90089, United States; orcid.org/0000-0002-7655-2907

Zezhi Wu – Ming Hsieh Department of Electrical and Computer Engineering, University of Southern California, Los Angeles, California 90089, United States

Yiyan Yu — Ming Hsieh Department of Electrical and Computer Engineering, University of Southern California, Los Angeles, California 90089, United States; orcid.org/0009-0000-5780-2803

Hee gon Kim − Ming Hsieh Department of Electrical and Computer Engineering, University of Southern California, Los Angeles, California 90089, United States; orcid.org/0009-0006-3945-0596

Juan Sanchez Vazquez – Ming Hsieh Department of Electrical and Computer Engineering, University of Southern California, Los Angeles, California 90089, United States

Chun-Ho Lee – Ming Hsieh Department of Electrical and Computer Engineering, University of Southern California, Los Angeles, California 90089, United States

Mengji Yu – Ming Hsieh Department of Electrical and Computer Engineering, University of Southern California, Los Angeles, California 90089, United States

Complete contact information is available at: https://pubs.acs.org/10.1021/acs.cgd.4c00116

Author Contributions

TH.U.C. and Z.W. contributed equally to this work. H.U.C., Z.W., and R.K. conceived the project and designed the experiments. H.U.C., Z.W., Y.Y., H.K., and J.S.V. performed the sample preparation and LT-TLP growth. H.U.C. performed the Hall measurement and EBSD characterization. H.U.C. and Z.W. performed PL and Raman characterization. All authors contributed to analyzing the data. H.U.C., Z.W.,

and R.K. wrote the paper, while all the authors provided feedback.

Notes

The authors declare no competing financial interest.

ACKNOWLEDGMENTS

This work was supported by the Department of Energy, Grant No. DE-SC0022248, the National Science Foundation, Award No. 2004791, the Office of Naval Research, Grant No. N00014-21-1-2634, and the Air Force Office of Scientific Research, Grant No. FA9550-21-1-0305.

REFERENCES

- (1) Rahim, A.; Ryckeboer, E.; Subramanian, A. Z.; Clemmen, S.; Kuyken, B.; Dhakal, A.; Raza, A.; Hermans, A.; Muneeb, M.; Dhoore, S.; et al. Expanding the silicon photonics portfolio with silicon nitride photonic integrated circuits. *J. Lightwave Technol.* **2017**, 35 (4), 639–649.
- (2) Nagarajan, R.; Joyner, C. H.; Schneider, R. P.; Bostak, J. S.; Butrie, T.; Dentai, A. G.; Dominic, V. G.; Evans, P. W.; Kato, M.; Kauffman, M.; et al. Large-scale photonic integrated circuits. *IEEE J. Sel. Top. Quantum Electron.* **2005**, *11* (1), 50–65.
- (3) Komljenovic, T.; Davenport, M.; Hulme, J.; Liu, A. Y.; Santis, C. T.; Spott, A.; Srinivasan, S.; Stanton, E. J.; Zhang, C.; Bowers, J. E. Heterogeneous silicon photonic integrated circuits. *J. Lightwave Technol.* **2016**, *34* (1), 20–35.
- (4) Rabiei, P.; Gunter, P. Optical and electro-optical properties of submicrometer lithium niobate slab waveguides prepared by crystal ion slicing and wafer bonding. *Appl. Phys. Lett.* **2004**, *85* (20), 4603–4605
- (5) Bazzan, M.; Sada, C. Optical waveguides in lithium niobate: Recent developments and applications. *Appl. Phys. Rev.* **2015**, 2 (4), No. 040603, DOI: 10.1063/1.4931601.
- (6) Qi, Y.; Li, Y. Integrated lithium niobate photonics. *Nano-photonics* **2020**, 9 (6), 1287–1320.
- (7) Zhu, D.; Shao, L.; Yu, M.; Cheng, R.; Desiatov, B.; Xin, C.; Hu, Y.; Holzgrafe, J.; Ghosh, S.; Shams-Ansari, A.; et al. Integrated photonics on thin-film lithium niobate. *Adv. Opt. Photonics* **2021**, *13* (2), 242–352.
- (8) Li, Z.; Wang, R. N.; Lihachev, G.; Zhang, J.; Tan, Z.; Churaev, M.; Kuznetsov, N.; Siddharth, A.; Bereyhi, M. J.; Riemensberger, J.; Kippenberg, T. J. High density lithium niobate photonic integrated circuits. *Nat. Commun.* **2023**, *14* (1), No. 4856.
- (9) Levy, M.; Osgood, R., Jr; Liu, R.; Cross, L.; Cargill, G., Iii; Kumar, A.; Bakhru, H. Fabrication of single-crystal lithium niobate films by crystal ion slicing. *Appl. Phys. Lett.* **1998**, 73 (16), 2293–2295.
- (10) Zhang, M.; Wang, C.; Cheng, R.; Shams-Ansari, A.; Lončar, M. Monolithic ultra-high-Q lithium niobate microring resonator. *Optica* **2017**, *4* (12), 1536–1537.
- (11) Fitzgerald, E. A.; Xie, Y. H.; Monroe, D.; Silverman, P.; Kuo, J.; Kortan, A.; Thiel, F.; Weir, B. Relaxed Ge x Si1- x structures for III-V integration with Si and high mobility two-dimensional electron gases in Si. *J. Vac. Sci. Technol.*, B **1992**, *10* (4), 1807–1819.
- (12) Passlack, M.; Zurcher, P.; Rajagopalan, K.; Droopad, R.; Abrokwah, J.; Tutt, M.; Park, Y.-B.; Johnson, E.; Hartin, O.; Zlotnicka, A. High mobility III-V MOSFETs for RF and digital applications. In 2007 IEEE International Electron Devices Meeting; IEEE 2007; pp 621–624.
- (13) Yin, Z.; Tang, X. A review of energy bandgap engineering in III–V semiconductor alloys for mid-infrared laser applications. *Solid-State Electron.* **2007**, *51* (1), 6–15.
- (14) Ning, C.-Z.; Dou, L.; Yang, P. Bandgap engineering in semiconductor alloy nanomaterials with widely tunable compositions. *Nat. Rev. Mater.* **2017**, 2 (12), No. 17070.
- (15) Park, M.-S.; Rezaei, M.; Nia, I.; Brown, R.; Bianconi, S.; Tan, C. L.; Mohseni, H. InGaAs/InP quantum well infrared photodetector

- integrated on Si substrate by Mo/Au metal-assisted wafer bonding. Opt. Mater. Express 2018, 8 (2), 413–419.
- (16) Chung, İ.-S.; Mørk, J. Silicon-photonics light source realized by III–V/Si-grating-mirror laser. *Appl. Phys. Lett.* **2010**, 97 (15), No. 151113, DOI: 10.1063/1.3503966.
- (17) Mauthe, S.; Baumgartner, Y.; Sousa, M.; Ding, Q.; Rossell, M. D.; Schenk, A.; Czornomaz, L.; Moselund, K. E. High-speed III-V nanowire photodetector monolithically integrated on Si. *Nat. Commun.* **2020**, *11* (1), No. 4565.
- (18) Tanabe, K.; Watanabe, K.; Arakawa, Y. III-V/Si hybrid photonic devices by direct fusion bonding. *Sci. Rep.* **2012**, *2* (1), No. 349.
- (19) Daix, N.; Uccelli, E.; Czornomaz, L.; Caimi, D.; Rossel, C.; Sousa, M.; Siegwart, H.; Marchiori, C.; Hartmann, J.; Shiu, K.-T.; et al. Towards large size substrates for III-V co-integration made by direct wafer bonding on Si. *APL Mater.* **2014**, 2 (8), No. 086104, DOI: 10.1063/1.4893653.
- (20) Bao, S.; Wang, Y.; Lina, K.; Zhang, L.; Wang, B.; Sasangka, W. A.; Lee, K. E. K.; Chua, S. J.; Michel, J.; Fitzgerald, E.; et al. A review of silicon-based wafer bonding processes, an approach to realize the monolithic integration of Si-CMOS and III–V-on-Si wafers. *J. Semicond.* **2021**, 42 (2), No. 023106.
- (21) Takigawa, R.; Higurashi, E.; Asano, T. Surface activated bonding of LiNbO3 and GaN at room temperature. *ECS Trans.* **2018**, 86 (5), 207.
- (22) Guo, Q.; Gutierrez, B. K.; Sekine, R.; Gray, R. M.; Williams, J. A.; Ledezma, L.; Costa, L.; Roy, A.; Zhou, S.; Liu, M.; Marandi, A. Ultrafast mode-locked laser in nanophotonic lithium niobate. *Science* **2023**, 382 (6671), 708–713.
- (23) Shams-Ansari, A.; Renaud, D.; Cheng, R.; Shao, L.; He, L.; Zhu, D.; Yu, M.; Grant, H. R.; Johansson, L.; Zhang, M.; Lončar, M. Electrically pumped laser transmitter integrated on thin-film lithium niobate. *Optica* **2022**, *9* (4), 408–411.
- (24) Sarkar, D.; Weng, S.; Yang, D.; Tao, J.; Naik, S.; Kale, S.; Chae, H. U.; Xu, Y.; Mesri, B.; Cronin, S. B.; et al. Low Temperature Growth of Crystalline Semiconductors on Nonepitaxial Substrates. *Adv. Mater. Interfaces* **2020**, *7* (14), No. 1902191.
- (25) Chae, H. U.; Shrewsbury, B.; Ahsan, R.; Ghanekar, A.; Povinelli, M. L.; Kapadia, R. Monolithic III—V on Metal for Thermal Metasurfaces. *ACS Nano* **2022**, *16* (11), 18497—18502.
- (26) Fenouillet-Beranger, C.; Beaurepaire, S.; Deprat, F.; de Sousa, A. A.; Brunet, L.; Batude, P.; Rozeau, O.; Andrieu, F.; Besombes, P.; Samson, M. Guidelines for intermediate back end of line (BEOL) for 3D sequential integration. In 2017 47th European Solid-State Device Research Conference (ESSDERC); IEEE, 2017; pp 252–255.
- (27) Deshpande, V.; Nair, K. S.; Holzer, M.; Banerjee, S.; Dubourdieu, C. CMOS back-end-of-line compatible ferroelectric tunnel junction devices. *Solid-State Electron.* **2021**, *186*, No. 108054.
- (28) Sarkar, D.; Wang, W.; Mecklenburg, M.; Clough, A. J.; Yeung, M.; Ren, C.; Lin, Q.; Blankemeier, L.; Niu, S.; Zhao, H.; et al. Confined liquid-phase growth of crystalline compound semiconductors on any substrate. *ACS Nano* **2018**, *12* (6), 5158–5167.
- (29) McCall, S. L.; Levi, A.; Slusher, R.; Pearton, S.; Logan, R. Whispering-gallery mode microdisk lasers. *Appl. Phys. Lett.* **1992**, *60* (3), 289–291.
- (30) Wong, W. W.; Jagadish, C.; Tan, H. H. III-V Semiconductor Whispering-Gallery Mode Micro-Cavity Lasers: Advances and Prospects. *IEEE J. Quantum Electron.* **2022**, 58 (4), 1–18.
- (31) Liu, H.; Zhang, Y.; Steenbergen, E. H.; Liu, S.; Lin, Z.; Zhang, Y.-H.; Kim, J.; Ji, M.-H.; Detchprohm, T.; Dupuis, R. D.; et al. Raman Scattering Study of Lattice Vibrations in the Type-II Superlattice InAs/InAs 1— x Sb x. *Phys. Rev. Appl.* **2017**, 8 (3), No. 034028.
- (32) Park, J. H.; Chung, C.-H. Raman spectroscopic characterizations of self-catalyzed InP/InAs/InP one-dimensional nanostructures on InP (111) B substrate using a simple substrate-tilting method. *Nanoscale Res. Lett.* **2019**, *14*, No. 355.
- (33) Veenhuizen, K.; McAnany, S.; Nolan, D.; Aitken, B.; Dierolf, V.; Jain, H. Fabrication of graded index single crystal in glass. *Sci. Rep.* **2017**, *7* (1), No. 44327.

- (34) Hackett, L.; Miller, M.; Weatherred, S.; Arterburn, S.; Storey, M. J.; Peake, G.; Dominguez, D.; Finnegan, P. S.; Friedmann, T. A.; Eichenfield, M. Non-reciprocal acoustoelectric microwave amplifiers with net gain and low noise in continuous operation. *Nat. Electron.* **2023**, *6* (1), 76–85.
- (35) Ghosh, S.; Cho, S.; Lu, R. Experimental Observation of Electron-Phonon Interaction in Semiconductor on Solidly Mounted Thin-Film Lithium Niobate. In 2022 IEEE MTT-S International Conference on Microwave Acoustics and Mechanics (IC-MAM); IEEE, 2022; pp 90–93.
- (36) Tao, J.; Sarkar, D.; Weng, S.; Orvis, T.; Ahsan, R.; Kale, S.; Xu, Y.; Chae, H. U.; Greer, F.; Ravichandran, J.; et al. High mobility large area single crystal III—V thin film templates directly grown on amorphous SiO2 on silicon. *Appl. Phys. Lett.* **2020**, *117* (4), No. 042103.
- (37) Wang, H.; Zeng, Y.; Fan, T.; Zhou, H.; Pan, D.; Dong, J.; Kong, M. Characteristics of InAs epilayers for Hall effect devices grown on GaAs substrates by MBE. *J. Cryst. Growth* **1997**, *179* (3–4), 658–660.
- (38) Singh, J. Electronic and Optoelectronic Properties of Semiconductor Structures; Cambridge University Press, 2007.
- (39) Palankovski, V.; Kaiblinger-Grujin, G.; Selberherr, S. Study of dopant-dependent band gap narrowing in compound semiconductor devices. *Mater. Sci. Eng., B* **1999**, *66* (1–3), 46–49.
- (40) Jain, A.; Sagar, P.; Mehra, R. Band gap widening and narrowing in moderately and heavily doped n-ZnO films. *Solid-State Electron.* **2006**, *50* (7–8), 1420–1424.
- (41) Gahlawat, S.; Singh, J.; Yadav, A. K.; Ingole, P. P. Exploring Burstein–Moss type effects in nickel doped hematite dendrite nanostructures for enhanced photo-electrochemical water splitting. *Phys. Chem. Chem. Phys.* **2019**, *21* (36), 20463–20477.
- (42) Reddy, R. R.; Anjaneyulu, S. Analysis of the Moss and Ravindra relations. *Phys. Status Solidi B* **1992**, *174* (2), K91–K93.
- (43) Chae, H. U.; Shrewsbury, B.; Ahsan, R.; Povinelli, M. L.; Kapadia, R. GaAs Mid-IR Electrically Tunable Metasurfaces. *Nano Lett.* **2024**, 24, 2581–2588, DOI: 10.1021/acs.nanolett.3c04687.
- (44) Wong, W. W.; Su, Z.; Wang, N.; Jagadish, C.; Tan, H. H. Epitaxially grown InP micro-ring lasers. *Nano Lett.* **2021**, *21* (13), 5681–5688.
- (45) Feng, L.; Wong, Z. J.; Ma, R.-M.; Wang, Y.; Zhang, X. Single-mode laser by parity-time symmetry breaking. *Science* **2014**, *346* (6212), 972–975.
- (46) Zhu, S.; Zhang, Y.; Ren, Y.; Wang, Y.; Zhai, K.; Feng, H.; Jin, Y.; Lin, Z.; Feng, J.; Li, S.; et al. Waveguide-Integrated Two-Dimensional Material Photodetectors in Thin-Film Lithium Niobate. *Adv. Photonics Res.* **2023**, *4*, No. 2300045.
- (47) Ahn, G. H.; White, A. D.; Kim, H.; Higashitarumizu, N.; Mayor, F. M.; Herrmann, J. F.; Jiang, W.; Multani, K. K.; Safavi-Naeini, A. H.; Javey, A.; Vučković, J. Platform-agnostic waveguide integration of high-speed photodetectors with evaporated tellurium thin films. *Optica* **2023**, *10* (3), 349–355.